Title
Geodetic Source Modeling of the 2019 Mw 6.3 Durrës, Albania, Earthquake: Partial Rupture of a Blind Reverse Fault

Journal
Geophysical Research Letters, 47(22)

ISSN
0094-8276

Authors
Govorčin, M
Wdowinski, S
Matoš, B
et al.

Publication Date
2020-11-28

DOI
10.1029/2020gl088990

Peer reviewed

Geodetic source modeling of the 2019, M_w 6.3 Durrës, Albania earthquake: partial rupture of a blind reverse fault

Enter authors here: M. Govorčin[1], S. Wdowinski[2], B. Matoš[3], and G. J. Funning[4]

[1]Faculty of Geodesy, University of Zagreb, Kačićeva 26, HR-10000 Zagreb, Croatia; marin.govorcin@geof.unizg.hr

[2]Department of Earth and Environment, Florida International University, 11200 SW 8th Street, Miami, FL 33199, USA; swdowins@fiu.edu

[3]Faculty of Mining, Geology and Petroleum Engineering, University of Zagreb, Pierottijeva 6, HR-10000 Zagreb, Croatia; bojan.matos@rgn.unizg.hr

[4]Department of Earth and Planetary Sciences, University of California, 900 University Ave., Riverside, CA 92521, USA; gareth.funning@ucr.edu

Corresponding author: M. Govorčin (marin.govorcin@geof.unizg.hr)

Key Points:

- Geodetic source modeling of the M_w 6.3 2019 Durrës earthquake based on Sentinel-1 DInSAR and GNSS observations
- A SW-dipping fault-plane agrees better with the seismic source parameters, depths, and locations of mainshock and aftershocks
- Rupture did not reach the surface, unruptured part of fault potentially poses elevated seismic hazard for the Albanian capital Tirana

Abstract

We address geometric and kinematic properties of the M_w 6.3, 26 November 2019 Durrës earthquake, the strongest earthquake in Albania in the past 40 years. Using coseismic surface displacements from Sentinel-1 DInSAR and nearby GNSS stations, we invert for the geometry and slip of the causative fault. We find that both a steep SW-dipping fault (dip 71°) and a shallow NE-dipping fault (dip 15°) can fit the data equally well. However, the slip on the SW-dipping fault occurs at depths (11-23 km), similar to the depths of the mainshock and aftershock seismicity, and thus we prefer that model. The location of our preferred fault-plane correlates with the mapped SW-dipping backthrust, the Vore fault. The fault rupture did not reach the surface, which implies that an up-dip stress propagation onto the unruptured shallow portion of the Vore fault and its secondary structures pose an increased seismic hazard for cities in Albania, including the capital, Tirana.

Plain Language Summary

The magnitude 6.3 earthquake near Durrës, Albania on November 26th, 2019 was the largest earthquake in the country for over 40 years. It caused 51 deaths and damaged over 2000 buildings in Durrës and the capital city Tirana. The earthquake occurred below the surface, and it was not immediately clear in the aftermath which fault it occurred on. We investigated that question using a combination of satellite observation techniques; DInSAR (a radar method that maps movements of the ground in one dimension over the large area) and GNSS (observations of three-dimensional movements of the ground at specific locations). Out of two possibilities, we prefer a model in which the earthquake occurred on a fault that steeply dips (tilts) to the southwest, between 11 and 23 km depth, agreeing with the depths of the mainshock and aftershocks from seismology. This fault, the Vore fault, is partly mapped at the surface, and runs close to Tirana. The upper 11 km of the Vore fault and its hangingwall structures did not move in this earthquake, and therefore they could still sustain a damaging earthquake in the future, threatening Tirana and other cities in northwestern Albania.

1 Introduction

The M_w 6.3 Durrës earthquake (26 November 2019; 03:54 CET; UTC+1) struck the coastal part of NW Albania near the city of Durrës, located 36 km west of the Albanian capital, Tirana. Its epicenter was located within the low terrain of the coastal Durrës depression (Figure 1a). The earthquake was felt all over Albania, southern Dalmatia (Croatia), southern Bosnia and Herzegovina, Montenegro, North Macedonia, SE Italy and NW Greece. It was the country's deadliest earthquake in the last 40 years. According to a report by Lekkas et al. (2019), 51 people died and nearly 2000 were injured in the event. The earthquake caused collapse or serious damage of more than 1,400 buildings in Tirana, and about 900 buildings in the city of Durrës and town of Thumanë (Figure 1b). Beside partial to complete failure due to shaking, a few buildings in the Durrës area were tilted due to liquefaction (Lekkas et al., 2019; Ormeni et al., 2020).

The M_w 6.3 Durrës event was the largest event of an earthquake sequence that began in mid-September 2019, roughly two months prior to the Durrës mainshock, and lasted for several months. The sequence included eight M>5 events, including M_w 5.6 and M_w 5.1 foreshocks (21 September 2019; 14:04 and 14:14 UTC, respectively), the M_w 6.3 Durrës mainshock, and five

M_w>5 aftershocks (Figure 1a) until March 31th, 2020. The series also included more than 17 M>4 aftershocks. Both the foreshock and mainshock events were at depths of around 20 km and 22 km, respectively, whereas the aftershock sequence occurred at depths of 10-30 km (Table S1). Focal mechanism solutions (FMS) for the Durrës mainshock, $M_w \geq 5$ foreshocks and four large aftershocks indicate thrust faulting mechanisms, consistent with active NW-SE-striking reverse fault structures mapped by geophysical subsurface explorations that either dip steeply to the SW or gently to the NE (Figure 1a,b; Aliaj, 2006; Velaj, 2015). These are consistent with the NE-SW-oriented maximum horizontal compressional stress (S_{Hmax}) for the region (Heidbach et al., 2016; Figure 1b).

The regional tectonics of NW Albania is dominated by the continental collision and subduction of the Adriatic microplate plate beneath Eurasia at a rate of 4-5 mm/yr (Serpelloni et al., 2013) and far-field effects of subduction along the Hellenic Arc (Biermanns et al., 2018; D'Agostino et al. 2020). These have form complex fold-and-thrust belts of the Dinarides-Albanides-Helenides orogens (Figure 1b; Biermanns et al., 2018), tectonically uplifted during the Cretaceous-Cenozoic orogeny (Schmid et al., 2020). Most of the strong earthquakes in NW Albania occur within the Ionian-Adriatic zone (IAZ; Figure 1a) (Aliaj et al., 2004). The IAZ acts as a contraction zone between the Albanian orogen (AB in Figure 1b) and the Adriatic foreland. The area is structurally complex, built of a series of regional NW-striking listric thrust sheets (*e.g.* the Lushnje fault) and their conjugate backthrusts (*e.g.*, the Vore fault) stretching southwestward into the Adriatic foreland basin (Schmid et al., 2008,2020). This is evidenced by strong seismicity mostly occurring on low-angle NE-dipping listric thrust sheets (*e.g.*, the M_w 7.1 1979 Montenegro earthquake; Baker et al. 1997) and rare occurrence of high-angle backthrust events (*e.g.*, Louvari et al. 2001; Copley et al. 2009), suggesting that regional backthrusts might play an important role in stress transfer along the Adriatic-External Albanides fold-and-thrust belt.

Based on the historic Albanian earthquake catalogue (Aliaj et al., 2010) the IAZ had several strong pre-instrumental events (*e.g.*,177 B.C.; 334 or 345 A.D; 506, 1273, and 1279 A.D.) and several strong M>6 earthquakes in the last few centuries, mostly in the period 1850-1900 (*e.g.*, 1869, 1870 and 1895) and the early 20th Century (*e.g.*, the M_s 6.2 1926 Durrës earthquake; Stucchi et al., 2012; Grunthal et al., 2013). Interestingly, based on its spatial distribution of shaking intensities, the 1926 Durrës earthquake showed similar macroseismic epicenter properties to the 2019 M_w 6.3 Durrës earthquake (Papazachos et al., 2011).

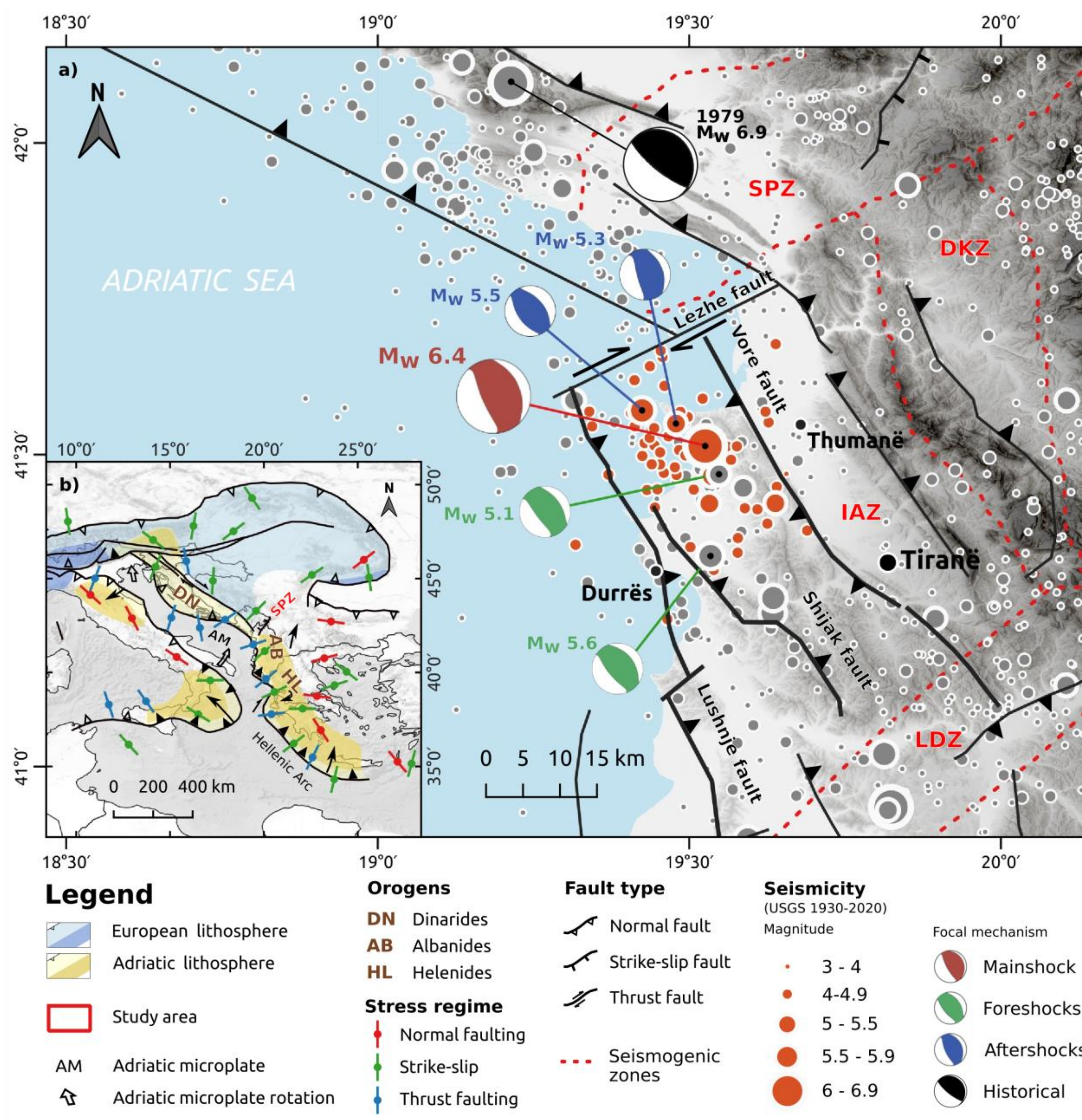

Figure 1. a) Map of seismic activity in NW Albania, showing M>3 events of the Durrës earthquake sequence with red circles, and pre-sequence events for the period 1930-2019 with grey circles. Focal mechanism solutions (FMS, Source USGS, 2020) are presented for the 2019 earthquake sequence of M>5 earthquakes (foreshocks: green, the mainshock: red, aftershocks: blue) and the $M_w \geq 6.9$ 1979 Montenegro earthquake (black; Source USGS, 2020). The map show locations of identified seismogenic zones and faults in the studied area (Aliaj et al 2014; Basili et al. 2013). Seismogenic zones in the studied area are indicated (SPZ: Shkoder-Peja Zone; DKZ: Drini-Ohri-Korca Zone; IAZ: Ionian-Adriatic Zone; LDZ: Lushnja-Elbasan-Diber Zone). Shaded relief is provided by ESRI World Hillshade Basemap data overlayed over SRTM 3 arc second digital terrain model. b) Regional tectonic framework of the study area (Handy et al. 2015) showing the subduction of Adriatic microplate lithosphere beneath European lithosphere, major orogens (Dinarides: DN, Albanides: AB, and Helenides: HL) and stress orientation. The SH_{max}

stress indications are primarily thrust and strike-slip faulting oriented NE-SW (Heidbach et al., 2016).

In this study, we use Differential Interferometric Synthetic Aperture Radar (DInSAR), Global Navigational Satellite System (GNSS), and seismic observations to estimate the coseismic slip induced by the 2019 Durrës earthquake and infer its geometric and kinematic properties. Our geodetic (DInSAR and GNSS) analysis relies on Sentinel-1 data acquired from both ascending and descending tracks, and data collected at two GNSS stations, respectively. The geodetic observations were inverted to estimate the geometry of the source fault, and the distribution of slip upon it, using half space elastic dislocation models (Okada, 1985), which we then use to discuss the effect that the Durrës event may have on local to regional fault systems. Similar geodetic-based studies of the M_w 6.3 Durrës earthquake were conducted by Ganas et al. (2020) and Caporali et al. (2020). However, these studies made *a priori* assumptions regarding the fault geometry and, hence, reached different results and conclusions than our study. The results of our study suggest a possible seismic hazard increase to cities in Albania, including the capital Tirana.

2 Geodetic Coseismic Observations

2.1 DInSAR

In this work, we use C-band Sentinel-1 SAR data from two ascending tracks (73 and 175) and one descending track (153) to form coseismic interferograms of the 2019 Durrës earthquake (Table S1). The Sentinel-1 satellite mission is a constellation of two C-band satellites Sentinel-1A (launched 2014) and Sentinel-1B (launched 2016) developed, launched, and operated by European Space Agency (ESA), as part of the European Union Copernicus space program. Sentinel-1 images were obtained in single look complex (SLC) format from the ESA and processed with the JPL/Caltech InSAR ISCE software (Rosen et al., 2018). We rely on Sentinel-1 precise orbits and a 3 arc-sec digital elevation model from the Shuttle Radar Topography Mission (SRTM; Farr et al., 2007) to geocode, coregister the SLC images, and remove topographic phase artifacts. The height of ambiguity of the interferometric pairs (Table S2) is over 100 m in all cases, resulting in a low sensitivity of the interferometric phase to topographic errors (typically on the order of 10 m for SRTM; Farr et al., 2007). We further apply an adaptive power-spectrum filter (Goldstein and Werner 1998) and unwrapping with the minimum cost flow SNAPHU algorithm (Chen and Zebker 2001). We apply a multilook ratio of 19:7 in range and azimuth directions to obtain ~90 m pixel posting of the geocoded interferograms. After geocoding, we use Generic Atmospheric Correction Online Service for InSAR (GACOS) data (Yu et al., 2018) to mitigate tropospheric phase delay in the geocoded interferograms (Figure S1). We then set the common unwrapping reference point at 41.88°N, 19.62°E for all interferograms. The selected location is in the far-field of the coseismic deformation zone and, hence, experienced a negligible amount of coseismic movement. The result are unwrapped interferograms, which are maps of coseismic surface displacements relative to the reference point in radar Line-of-Sight (LOS).

DInSAR processing of the three coseismic pairs (Table S2) yielded three coseismic interferograms, one descending track and two ascending tracks (Figure 2). All three interferograms yield concentric fringe patterns centered ~6 km north-northeast of the epicenter location (Figure 2 a,b,c). Both east- and west-looking (ascending and descending) interferograms show the same sense of displacement - toward the satellite - implying mostly vertical ground displacements. The maximum LOS displacements are 10 and 6 cm (3 and 2 fringe cycles) in ascending and descending track interferograms, respectively (Figure 2 d,e,f), located 18 km northeast of the city of Durrës and 16 km southwest of the town of Thumanë. We consider any contributions of interseismic and postseismic signal to be negligible due to the short time-span (6-12 days) of the interferometric pairs covering the mainshock. The amplitude (6-10 cm) and area coverage (790 km^2) of the observed coseismic deformation are compatible with a deep seismic source.

2.2 GNSS

GNSS data used in this study were collected by the Albanian GNSS network (ALBOS) at two permanent stations Tirana (TIR4), and Durres (DUR2), located 37 km southeast and 24 km southwest of the mainshock's epicenter, respectively. We use two month-long time series of a daily (24 hour) GNSS position solution centered on the mainshock date, calculated by the Nevada Geodetic Laboratory in the IGS14 reference frame (Blewett et al., 2018), to estimate coseismic offsets. For each component time series, we fit a Heavyside step function embedded in a linear curve with a given slope determined by the long-term trend of the positioning change (Figure S2), as calculated by the MIDAS algorithm (Blewitt et al., 2018). Our GNSS-derived coseismic offsets show horizontal ground movements of 0.6 cm and 2.6 cm in SW direction, and vertical ground movements of -0.3 cm and +1.3 cm at TIR4 and DUR2 , respectively (Figures 2 d,e,f and S2).

To compare the GNSS and DInSAR coseismic displacements, we project the GNSS displacements into the LOS acquisition geometries of the three SAR tracks (153, 175, and 73). We find good agreement (0.06-0.40 cm) between LOS displacements at DUR2 and less good agreement (0.30-1.80 cm) at TIR4 (Table S3). The largest disagreement (1.82 cm) can be found between DInSAR T175 and TIR4 LOS displacements, whereas DInSAR T153 and T73 still show a relatively good agreement (~0.5 cm) with TIR4. These differences most likely reflect noise due to tropospheric turbulence in the SE part of the study area, even after the GACOS corrections. Considering that this area is outside of the main DInSAR coseismic deformation pattern (Figure 2), the observed disagreement between DInSAR T175 and TIR4 should not significantly affect the inversion results.

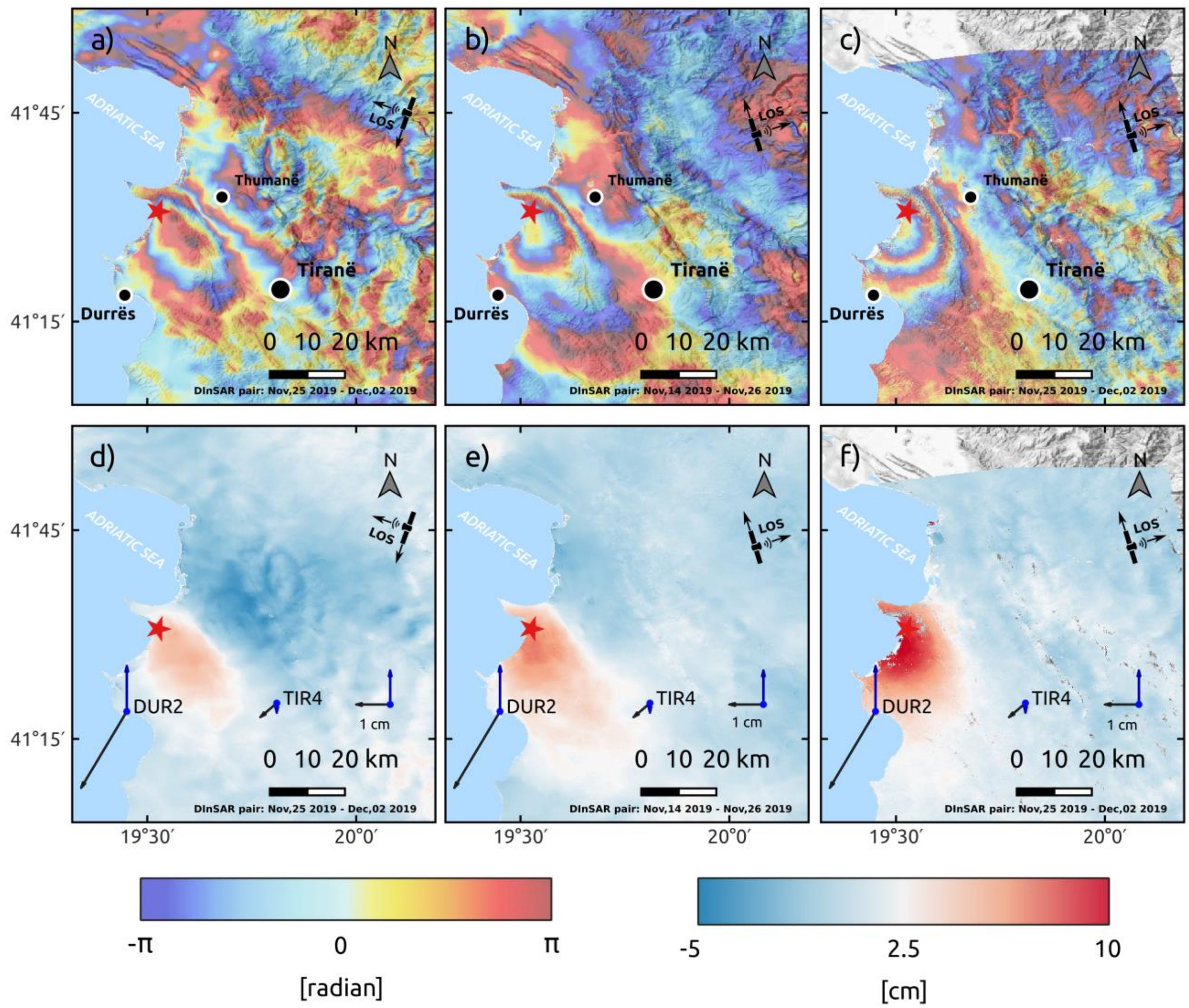

Figure 2. Sentinel-1 wrapped interferograms and unwrapped displacement maps of the coseismic deformation induced by the 2019 Durrës earthquake. One interferogram is from a descending track 153 (a) and two are from ascending tracks 175 (b) and 73 (c). The unwrapped displacement maps are presented beneath the interferograms. Red stars mark the Durrës earthquake epicenter location (Source: USGS, 2020). Black and blue arrows represent GNSS-detected horizontal and vertical coseismic displacements, respectively. Positive displacements and phase gradients indicate relative motion of the ground towards the satellite (range decrease) in LOS direction.

3 Coseismic Dislocation Modeling

In order to infer the location, fault geometry and slip distribution of the 2019 M_w 6.3 Durrës earthquake, we model rectangular dislocations in an elastic half space (Okada, 1985) to estimate the earthquake source parameters that produced the observed DInSAR and GNSS coseismic displacements. For this, we employ a two-step approach: non-linear optimization for the best-fitting fault geometries and location with uniform slip (Section 3.1) followed by non-negative linear inversion for the slip distribution on those fault geometries (Section 3.2).

Before the modeling, we use an adaptive gradient-based quadtree sampling algorithm (Decriem et al., 2010) to down-sample the DInSAR coseismic data to increase the computational efficiency of the inversions. This reduced the number of data points from several million to around 1000 points per dataset (Figure S3), concentrated in the area with the largest displacement gradients. In both steps, the inversions were weighted using the weighting matrix constructed from the variance of GNSS displacements (Figure S2) and a variance-covariance matrix of DInSAR coseismic displacements. We estimate the variance-covariance matrix based on an exponential semivariogram calculated over a non-deforming area (*e.g.*, Bagnardi and Hooper, 2018). We choose to equally weight DInSAR and GNSS datasets as we find that upscaling the GNSS weights results in an insignificant GNSS fit improvements at an expense of increased misfit with DInSAR (Figure S4). Additional terms consisting of linear ramps and constant offsets for DInSAR dataset are included in the inversions; these allow the inversions to estimate residual long wavelength errors due to orbital errors and/or atmospheric noise, and any displacement offsets between datasets.

3.1 Fault geometry inversion

The first, we perform a non-linear inversion step with the Geodetic Bayesian Inversion Software (GBIS; Bagnardi and Hooper, 2018), which employs a Metropolis-Hastings Markov Chain Monte Carlo (MCMC) algorithm to estimate the posteriori probability distribution for all parameters of regular elastic dislocation (Okada, 1985). The optimal dislocation model is found based on the posterior probabilities estimated from 1 million MCMC sampling iterations of each model parameter. We constrain an inversion search parameter space with the range of FMS parameters (Strike, Dip, Rake; Table 1) estimated for the mainshock and aftershocks by various published sources (Table S1). Both SW and NE-dipping fault planes are tested to find which fault plane solution better describes the observed coseismic deformation.

We find that the root-mean-square error (RMSE) misfit of the model for the SW-dipping plane is marginally smaller (0.87 cm) than that of the model for the NE-dipping plane (0.89 cm). Both models show a slightly greater misfit with the DInSAR displacement map from track 175, compared to the other displacement maps (Table S5). This is also reflected in the comparison with GNSS data, which suggests that T175 displacement map contains some unmodeled tropospheric noise in the SE of the study area (Figure S7). The models also show very good fits at DUR2, but poor at TIR4 GNSS station in both cases (Figure S8). The optimal models suggest that the rupture area for the NE-dipping plane is significantly larger (266 km^2) than the rupture area for the SW-dipping plane (121 km^2), although the models present similar geodetic moments. Using a shear modulus of 30 GPa, we estimate the moments of 4.35×10^{18} Nm (M_w 6.36) and 4.23×10^{18} Nm (M_w 6.36) for the SW- and NE-dipping planes, respectively. Both models suggest that the top of the rupture plane is situated at around 14 km depth. Bayesian inversions in both cases show roughly Gaussian distributions for all fault source parameters and slight trade-offs between fault width and slip parameters with minor changes of depth (Figures S5 and S6). Thus, we test how the inversion would perform with fixed fault width starting from 4 to 20 km in 2 km increments (Table S4). Beside the expected variation of slip and depth parameters, we find that the strike, dip and rake for both planes (Table S4) correspond well to the ranges from FMS (Table S1). At the same time, all optimal NE-dipping models describe a fault plane that extends down to around 16 km depth, whereas the SW-dipping fault planes extend to around 26 km depth. The latter suggests that models for the SW-dipping plane correspond better to the reported FMS depth of the mainshock (~ 22 km) and the strongest aftershocks (Table S1).

Table 1. Green function parameters search intervals for MCMC sampling and an obtained optimal model for the SW and NE-dipping fault plane solution from non-linear uniform slip inversion with associated root-mean-square error, and geodetic moment

Orient.	Inver.	Length (km)	Width (km)	Depth[a] (km)	Lon (°)[b]	Lat (°)[b]	Strike (°)	Dip (°)	Rake (°)	Slip (cm)	RMSE (cm)	M_o x10^{18} Nm
SW	Bounds	1-30	1-20	1-26	19.27 - 19.74	41.25 - 41.62	125-175	50-90	60-100	0-150	-	-
	Optimal	18.83 ±2.3	6.41 ±3.1	14.11 ±1.1	19.59 ±0.01	41.52 ±0.01	150 ±1.5	71 ±2.2	70 ±4.7	120 ±27	0.87	4.35
NE	Bounds	1-30	1-20	1-26	19.27 - 19.74	41.25 - 41.62	330-380 (20)	1-40	80-140	0-150	-	-
	Optimal	21.38 ±2.2	12.43 ±1.9	13.45 ±0.9	19.53 ±0.01	41.50 ±0.01	348 ±5.6	15 ±2.2	111 ±6.1	53 ±16	0.89	4.23

[a] Depth parameter points to the top of fault plane [b] Lon, Lat represent coordinates of the top fault plane midpoint projected on the surface

3.2 Slip inversion

The best-fit slip distribution is estimated using a smoothed linear inversion solved by a non-negative least square algorithm described in Funning et al. (2005). The initial geometries for both SW- and NE-dipping fault planes are obtained from the uniform slip inversion (Table 1). We extend the fault planes to length of 36 km and widths of 20 km to allow the inversion to constrain the extent of the fault slip in both cases. These extended fault planes are discretized into 1 x 1 km patches (720 fault segments). We then solve for the slip of each element that best fits the data in a non-negative least squares sense, while testing different values of a Laplacian smoothness parameter. We choose the preferred slip models for each geometry on the basis of a trade-off L-curve (Figure S9), visually selecting the model at the smoothness value where data-to-model misfit decreases significantly (*i.e.*, the smoothest model that fits the data well). The preferred slip model for the SW-dipping fault indicates that most slip is confined between 11 and 23 km, peaking at 119 cm at depth of 17 km depth (Figure 3c). The preferred NE-dipping model shows slip between 13 and 17 km depth, with a peak of 114 cm at 15 km depth (Figure 3d). Both models show elongated slip distributions to the north, along the strike of the fault plane. This corresponds well with the aftershock distribution (Figure 3a,b), being located to the north / northeast of the mainshock epicenter. The obtained total rupture area (fault segments with slip > 0.12 m) with distributed slip models are 238 km^2 and 218 km^2 for the SW- and NE-dipping planes, respectively.

A comparison between geodetic and distributed-slip modeled displacement misfits (Table S5 and Figures S9,S10) indicate that (1) the models fit the GNSS results better than the DInSAR, and (2) the SW-dipping model better fits the GNSS observations than the NE-dipping model. The RMSE of the overall misfit between geodetic data and the models is ~0.73 cm showing an overall good fit in both cases (Figure S10, S11, and Table S5). Comparisons with various earthquake catalogues (Table S6) indicate that the SW-dipping model a agrees with the mainshock FMS locations (Figure S13), especially the IGEWE, GFZ and USGS solutions, better than the NE-dipping model. The best overall agreement is observed with the USGS solution which is displaced 7.2 ± 4.8 km horizontally and 2.5 ± 1.8 km in depth from the obtained SW-dipping centroid. In addition, the USGS mainshock hypocenter depth agrees quite well with the bottom depth of the SW-dipping model slip distribution (Figure 3c). The foreshock and aftershock distribution may suggest the activation of secondary fault structures in this earthquake sequence (Figure 3a,c). However, the geometry of the seismic activity in the earthquake sequence is unreliable for a more detailed analysis on the transects (Figure 3c,d), as most of the smaller earthquakes are determined with fixed depth and cannot be used in the analysis, whereas a precise relocation was outside of the scope of this study.

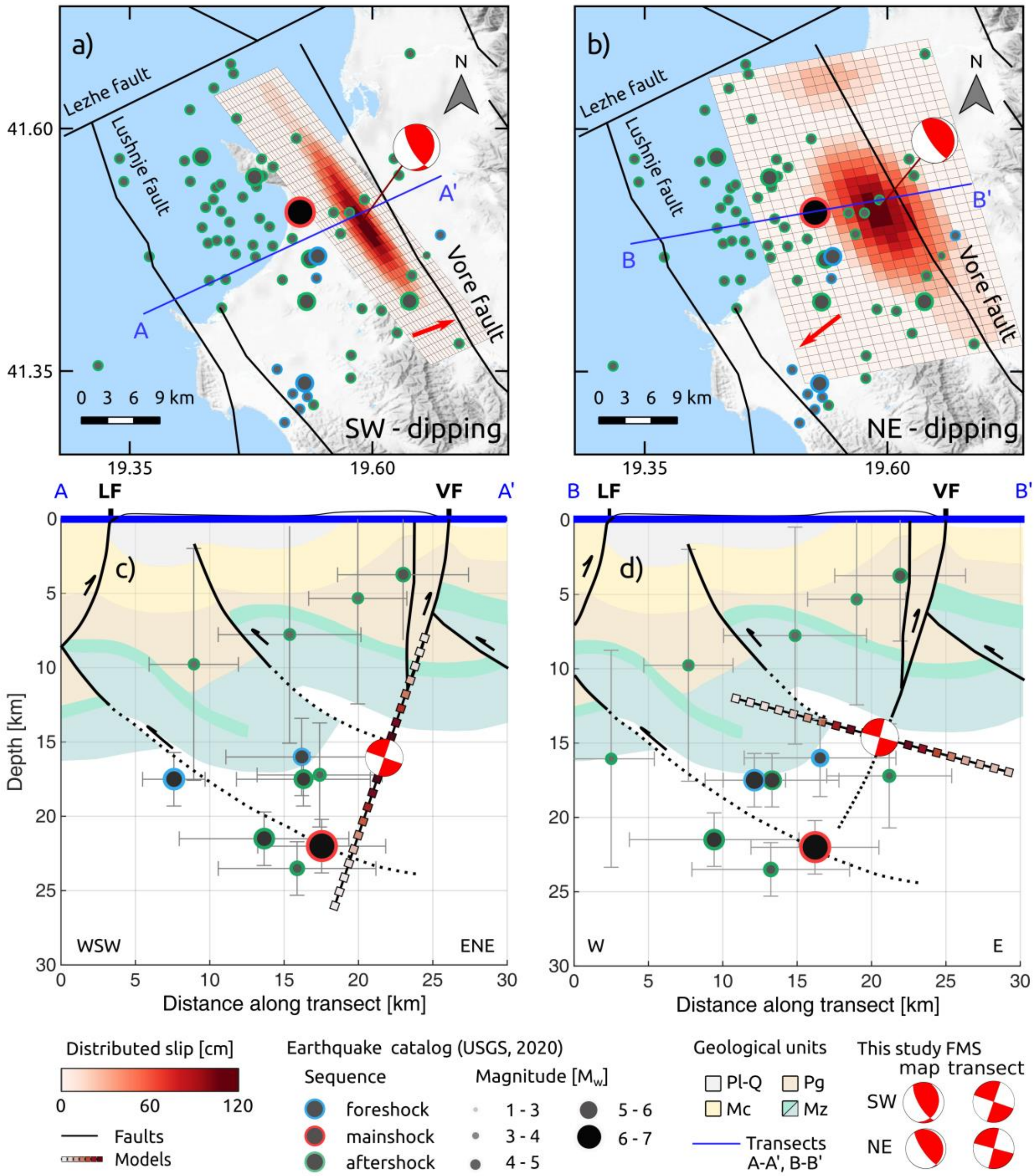

Figure 3. a) and b) represent map views of the two distributed slip models with the epicentre locations (circles with a red stroke: mainshock, blue: foreshock, green: aftershock; Source USGS 2020) Black lines mark the surface trace of seismogenic faults (Source; Aliaj et al 2014 and Basili et al. 2013) and blue line mark the location of vertical seismicity transects presented in c) and d). Red arrows represent the model slip rake vectors. c) and d) are vertical transects oriented normal to the dip of the tilted distributed slip models showing the fault trajectory (black lines with colored squares; color represents slip value), earthquake hypocenters (circles), and geological settings constructed after Xhomo et al. (1999), Aliaj (2006), Silo et al. (2010) and Velaj (2015) with surface traces of mapped faults (LF-Lushnje fault, VF- Vore fault),

andgeological units: Pl-Q: Pliocene-Quaternary sediments, Mc: Miocene molasse sediments, Pg: Paleogene flysch and limestones, and Mz: mesozoic carbonates, cherts and siliciclastics. The hypocenters with fixed depths (10 km) are excluded from the analysis on the transects, whereas the location uncertainties are shown as gray error bars. Red FMS represent mechanisms and centroides of mainshock models obtained in this study.

4 Discussion

This paper presents both uniform and distributed slip models of the 2019, M_w 6.3 Durrës earthquake, which was the strongest earthquake event in Albania in the past 40 years. Our two-step inversions of geodetic displacements revealed two possible models, with SW- and NE-dipping fault planes. We could not unambiguously find a preferred optimal rupture plane just based on the geodetic data-to-model misfit, as models for both fault planes fit the data equally well (misfit <1 cm). Caporali et al. (2020), Ganas et al. (2020), and Papadopoulos et al. (2020) propose and model only the NE-dipping fault as a causative fault primarily based on the interpretation of the regional structural settings. A similar mechanism for the NE-dipping fault are presented but with different centroid depths and coseismic slip values, mostly due to an applied inversion method with certain assumptions (Table S7). Therefore, the results of these studies could be biased, especially as the available geological-geophysical subsurface data indicate existence of both subsurface thrust and backthrust faults which may be both interpreted as a source of the Durrës mainshock at their deeper section (Figure 3c,d).

In addition, by comparison with various earthquake catalogues, we find that the obtained fault geometry, location and depth range of the SW-dipping model agrees better with the earthquake sequence and the depth ranges of various mainshock FMSs (Figures 3c, S13) than the NE-dipping model. Moreover, a postseismic deformation pattern seems to also be more suggestive of a steeply-dipping fault than a shallow one (Figure S13), and the optimal mechanism of the SW-dipping fault plane (Strike: 150°, Dip 71°, Rake 70°) corresponds well to the reported mean FMS parameters (Strike: 147°, Dip 71°, Rake 84°) for the Durrës mainshock (Table S1). Thus, we suggest that the 2019 M_w 6.3 Durrës earthquake rupture most likely occurred on the SW-dipping backthrust Vore fault (Figure 3a,c) characterized by reverse motion with a minor sinistral component.

Our preferred model together with the seismicity data suggest that the mainshock rupture started at ~22 km depth on the SW-dipping Vore fault (Figure 3c) and propagated upwards along the fault plane to ~17 km depth, where the most accumulated stress was released. The best-fitting distributed-slip model shows a rupture area of 238 km^2 confined between 11 km and 23 km depth with peak slip of 119 cm (Figure 3c), and a geodetic moment of 3.79×10^{18} Nm (M_w 6.33). This corresponds well to the reported seismic moment magnitudes from FMS (Table S1) and a seismogenic layer assumed to be in the range of 11 to 26 km depth (Copley et al. 2009). In addition, our slip vector agrees well with the direction of active shortening in the IAZ (D'Agostino et al. 2020).

The high-angle SW-dipping backthrusts, such as the Vore fault, are formed under the influence of the Upper Triassic evaporite layers in the Adriatic-External Albanides fold-and-thrust belt. These faults partly accommodate compressional stresses caused by an ongoing convergence of the Adriatic foreland along the External Albanides (D'Agostino et al. 2020), which is evidenced by high-angle thrust events (Muco 1994) that usually coincide with anticlines on the surface (Copley et al. 2009). We find this to be in agreement with our preferred causative fault plane as its location agrees with the cogenetic Mio-Pliocene NW-SE striking asymmetric Vore anticline structure (Velaj, 2005, Xhomo et al. 1999,2002). Similar thrust salt-tectonic conditions with high-angle thrust faults can be found in the Zagros fold-and-thrust belt (Nissen et al. 2010, 2011).

We find it interesting that the reported foreshock and majority of aftershock epicenters are dispersed and located to the west of the preferred mainshock fault plane. This could imply a possible activation of secondary structures in this earthquake sequence. However, a detailed analysis of activated structures is not possible due to incompleteness and limitations of the available earthquake catalog.

Our study shows that the coseismic slip was arrested at 11 km depth and did not reach the surface, which agrees with field observations (Lekkas et al. 2019). This implies that a shallower part of the Vore fault, its SE segment, and potentially its hangingwall secondary structures from 11 km to the surface (Aliaj, 2006) did not rupture. If deformation in this updip zone were accommodated aseismically, *e.g.*, through creep, we would expect to see evidence of this as a sharp discontinuity in postseismic interferograms, but we do not (Figure S12).

The updip structures were likely brought closer to failure with up-dip stress transfer from the mainshock, and consequently pose an elevated seismic hazard for the Tirana metropolitan area. Using Coulomb stress failure changes induced by a slip on either the SW- or NE-dipping faults, we calculate a mean failure stress increase between 0 and 25 km depth projected onto the rupture fault plane with an assumed effective friction coefficient of 0.4. The results show that the southern part of the Vore fault, passing near the city of Tirana, is loaded with a stress in the range 0.2 – 0.5 MPa from the rupture of either possible solution (Figure S14). In addition, the 5 km thick Neogene-Quaternary sediment succession of the Tirana depression (Aliaj, 2006) additionally increases local seismic hazard due to its weak mechanical properties and the likelihood of seismic wave amplification. The distribution of available aftershocks and the SW-dipping distributed-slip model reflects the likely slip propagation in the mainshock to the north-northwest, towards the NE-striking strike-slip Lezhe fault (Figure 3a). This could further be indicative of increased seismic hazard in NW Albania and SE Montenegro due to partial stress transfer of 0.4 MPa and possible stress accumulation along the Lezhe fault towards the Shkoder-Peja transverse seismogenic zone (Figure 1a, Figure S14), whose last strong earthquakes, M 6.6 and M 5.6 events, occurred in 1905 and 1948 respectively (Aliaj et al. 2010).

5 Conclusions

We determined the coseismic displacement field of the M_w 6.3 Durrës mainshock using three differential interferograms from the Sentinel-1 satellite mission and GNSS time-series data at two GNSS stations in the vicinity of the mainshock epicentre. The comparison between inverse models fitted to geodetic coseismic displacements and seismic data suggest that the seismogenic source for the Durrës earthquake was probably the 71° SW-dipping Vore backthrust fault. The best-fitting model of distributed slip for the Durrës earthquake involved slip between 11 and 23 km depth and did not reach the surface. This implies that the shallow part of the Vore fault, *i.e.*, the blind segment and hangingwall secondary structures, above 11 km depth have been brought closer to the failure, which presents an elevated seismic hazard for the Albanian capital Tirana. Our results suggest that there may be also a partial stress transfer to the Shkoder-Peja transverse seismogenic zone, which last experienced an M>5.5 earthquake in 1948.

Acknowledgments, Samples, and Data

- We acknowledge the free access to satellite images and GNSS time-series data provided by the European Space Agency, Albanian GNSS network (ALBOS) and Nevada Geodetic Laboratory, respectively, to perform the analysis and modeling of the M_w 6.3 Durrës earthquake
- Data used in this research; (1) Sentinel-1 SAR images are available through Copernicus Open Access Hub website (https://scihub.copernicus.eu/dhus/#/home) , (2) topographic phase delay maps are available through Generic Atmospheric Correction Online Service website (GACOS; http://ceg-research.ncl.ac.uk/v2/gacos/), (3) GNSS time-series data is available through Nevada Geodetic Laboratory website (http://geodesy.unr.edu/NGLStationPages/gpsnetmap/GPSNetMap.html), (4) Focal Mechanism Solutions are available at U.S. Geological Survey (USGS; https://earthquake.usgs.gov/earthquakes/search/), Global Centroid Moment Tensor Catalog (GCMT; https://www.globalcmt.org/CMTsearch.html), German Research Centre for Geosciences (GFZ; https://geofon.gfz-potsdam.de/eqinfo/list.php), Institute of GeoSciences, Energy, Water and Environment (IGEWE; https://www.geo.edu.al/newweb/?fq=sizmobuletinet&gj=gj2&kid=36), Institut de Physique du Globe de Paris (IPGP; http://geoscope.ipgp.fr/index.php/en/), and Regional Centroid Moment Tensor (RCMT; http://rcmt2.bo.ingv.it/) website, (5) Earthquake catalogs are available at the SHARE European Earthquake Catalog (https://www.emidius.eu/SHEEC/) and U.S. Geological Survey (USGS; https://earthquake.usgs.gov/earthquakes/search/) website, (6) fault data is available at the European Database of Seismogenic Faults website (http://diss.rm.ingv.it/share-edsf/) and through Aliaj et al 2014, (7) regional tectonic framework is available through Handy et al. 2015, (8) SH_{max} stress indications are available through Heidbach et al., 2016, and (9) topography hillshade map used in the Figures 1,2,3 is available through ESRI website (https://www.arcgis.com/home/item.html?id=1b243539f4514b6ba35e7d995890db1d).
- The authors declare no conflict of interest

References

Aliaj, S., Kociu, S., Muco, B., & Sulstarova, E. (2010). Seismicity, seismotectonics and seismic hazard assessment in Albania. *Albanian Academy of Sciences*, Tirana

Aliaj S. (2006). The Albanian orogen: Convergence zone between Eurasia and the Adria microplate. *The Adria Microplate: GPS Geodesy, Tectonics and Hazards*, Nato Science Series: IV: Earth and Environmental Sciences, 61. 133-149. Springer, Dordrecht, https://doi.org/10.1007/1-4020-4235-3_09

Aliaj, S., Adams, J., Halchuk, S., Sulstarova, E., Peci, V., & Muco, B., (2004). Probalistic seismic hazard maps for Albania. Paper presented at *13th World Conference on Earthquake Engineering*,Vancouver, B.C., Canada, https://doi.org/10.4095/226354

Bagnardi, M. & Hooper, A. (2018). Inversion of surface deformation data for rapid estimates of source parameters and uncertainties: A Bayesian approach. *Geochemistry, Geophysics, Geosystems*, 19, 2194-2211, https://doi.org/10.1029/2018GC007585

Baker, C., Hatzfeld, D., Lyon-Caen, H., Papadimitriou, E., & Rigo, A. (1997). Earthquake mechanisms of the Adriatic Sea and Western Greece implications for the oceanic subduction-continental collision transition. *Geophysical Journal International*, 131(3), 559-594, https://doi.org/10.1111/j.1365-246X.1997.tb06600.x

Basili R., Kastelic V., Demircioglu M. B., Garcia Moreno D., Nemser E. S., Petricca P., et al.(2013). The European Database of Seismogenic Faults (EDSF) compiled in the framework of the Project SHARE. http://diss.rm.ingv.it/share-edsf/ , doi: 10.6092/INGV.IT-SHARE-EDSF

Biermanns, P., Schmitz, B., Ustaszewski, K., & Reicherter, K., (2018). Tectonic geomorphology and Quaternay landscape development in Albania-Montenegro border region: An inventory. *Geomorphology*, 326, 116-131, https://doi.org/10.1016/j.geomorph.2018.09.014

Blewitt, G., Hammond, W. C. & Kreemer, C. (2018). Harnessing the GPS data explosion for interdisciplinary science. *Eos*, 99, https://doi.org/10.1029/2018EO104623

Caporali, A., Floris, M., Chen, X., Nurce, B., Bertocco, M., & Zurutuza, J. (2020). The November 2019 Seismic Sequence in Albania: Geodetic Constraints and Fault Interaction, *Remote Sensing*, 12 (5) 846, https://doi.org/10.3390/rs12050846

Chen, C. W. & Zebker, H. A. (2001). Two-dimensional phase unwrapping with use of statistical models for cost functions in nonlinear optimization. *Journal of Optical Society of America A*, 18(2), 338-351, https://doi.org/10.1364/JOSAA.18.000338

Copley, A., Boait, F., Hollingsworth, J., Jackson, J., & McKenzie, D. (2009). Subparallel thrust and normal faulting in Albania and the roles of gravitational potential energy and rheology contrasts in mountain belts. *Journal of Geophysical Research: Solid Earth*, 114, B5. https://doi.org/10.1029/2008JB005931

D' Agostino, N., Metois, M., Koci, R., Duni, L., Kuka, N., Ganas, A., et al. (2020). Active crustal deformation and rotations in the southwestern Balkans from continuous GPS measurements, *Earth and Planetary Science Letters*, 539, 116246, https://doi.org/10.1016/j.epsl.2020.116246

Decriem, J., Arnadottir, T., Hooper, A., Geirsson, H., Sigmundsson, F., Keiding, M., et al. (2010). The 2008 May 29 earthquake doublet in SW Iceland. *Geophysical Journal International*, 181 (2) 1128-1146, https://doi.org/10.1111/j.1365-246X.2010.04565.x

Farr, T. G., Rosen, P. A., Caro, E., Crippen, R., Duren, R., Hensley, S., et al. (2007). The shuttle radar topography interferometry mission. *Reviews of geophysics*, 45(2), https://doi.org/10.1029/2005RG000183

Funning, G. J., Parsons, B., Wright, T. J., Jackson, J. A., & Fielding, E. J. (2005), Surface displacements and source parameters of the 2003 Bam (Iran) earthquake from Envisat advanced synthetic aperture radar imagery. *Journal of Geophysical Research: Solid Earth*, 110, B09406, https://doi.org/10.1029/2004JB003338

Ganas, A., Elias, P., Briole, P., Cannavo F., Valkaniotis, S., Tsironi, V., & Partheniou, E. I., (2020), Ground Deforation and Seismic Fault Model of the M6.4 Durres (Albania) Nov. 26, 2019 Earthquake, Based on GNSS/INSAR Observations. *Geosciences*, 10, 210, https://doi.org/10.3390/geosciences10060210

GCMT, Global Centroid Moment Tensor Catalog (GCMT) Available from: https://www.globalcmt.org/CMTsearch.html (Accessed on 15 May 2020)

GFZ, German Research Centre for Geosciences, GEOFON program, Available from: https://geofon.gfz-potsdam.de/eqinfo/list.php (Accessed on 15 May 2020)

Grunthal, G., Wahlstrom, R., & Stromeyer, D. (2013). The SHARE European Earthquake Catalogue (SHEEC) for the time period 1900-2006 and its comparison to the European-Mediterranean Earthquake Catalogue (EMEC). *Journal of Seismology*, 17, 4, 1339-1344, https://doi.org/10.1007/s10950-013-9379-y

Goldstein, R. M. & Werner, C. L. (1998). Radar interferogram filtering for geophysical applications. *Geophysical Research Letters*, 25(21), 4035-4038, https://doi.org/10.1029/1998GL900033

Handy, M. R., Ustaszewski, K., & Kissling, E. (2015). Reconstructing the Alps-Carpathians-Dinarides as a key to understanding switches in subduction polarity, slab gaps and surface motion. *Internationl Journal of Earth Sciences* (Geol Rudsch), 104,1-26, https://doi.org/10.1007/s00531-014-1060-3

Heidbach, O., Custodio, S., Kingdon, A., Mariucci, M.T., Montone, P., Müller, B., et al. (2016). Stress Map of the Mediterranean and Central Europe 2016. *GFZ Data Service*, http://doi.org/10.5880/WSM.Europe2016

IGEWE, Institute of GeoSciences, Energy, Water and Environment (IGEWE), Polytechnic University of Tirana (Albania), Seismologic bulletin, Available from: https://www.geo.edu.al/newweb/?fq=sizmobuletinet&gj=gj2&kid=36 (Accessed on 15 May 2020)

IPGP, Institut de Physique du Globe de Paris (IPGP), GEOSCOPE observatory, Available from: http://geoscope.ipgp.fr/index.php/en/ (Accessed on 15 May 2020)

Lekkas, E., Mavroulis, S., Papa, D., & Carydsi, P. (2019). The November 26, 2019 Mw 6.4 Durres (Albania) earthquake. *Newsletter of Environmental Disaster and Crises Management Strategies*, 15, ISSN 2653-9543.

Louvari, E., Kiratzi, A., Papazachos, B., & Hatzidimitriou, P. (2001). Fault-plane Solutions Determined by Waveform Modeling Confirm Tectonic Collision in the Eastern Adriatic. *Pure and Applied Geophysics.* 158, 1613-1637, https://doi.org/10.1007/PL00001236

Muco, B. (1994). Focal mechnism solutions for Albanian earthquakes for the years 1964-1988, *Tectonophysics.* 231, 311-323, https://doi.org/10.1016/0040-1951(94)90041-8

Nissen, E., Yamini-Fard, F., Tatar, M., Gholomazadeh, A., Bergman, E., Elliott, J.R., Jackson, J.A., Parsons, B. (2010). The vertical separation of mainshock rupture and microseismicity at Qeshm island in the Zagros fold-and-thrust belt, Iran. *Earth and Planetary Science Letters*, 296 (3-4), 181-194, https://doi.org/10.1016/j.epsl.2010.04.049

Nissen, E., Tatar, M., Jackson, J.A., & Allen, M.B. (2011). New views on earthquake faulting in the Zagros fold-and-thrust belt of Iran. *Geophysical Journal International*, 186 (3) 928-944, https://doi.org/10.1111/j.1365-246X.2011.05119.x

Okada, Y. (1985). Surface deformation due to shear and tensile faults in a half-space. *Bulletin of Seismological Society of America*, 78(4), 1438-1449.

Ormeni, R., Hoxha, I., Naco, P., & Gego, D. (2020). The strong earthquake of 26 November 2019 (MW6.4) and its associate active tectonic of Durresi Region in Albania. Paper presented at *EGU General Assembly 2020* -6096, https://doi.org/10.5194/egusphere-egu2020-6096

Papadopoulos, G. A., Agalos, A., Carydis, P., Lekkas, E., Mavroulis, S., & Triantafyllou, I. (2020). The 26 November 2019 Mw 6.9 Albania Destructive Earthquake. *Seismological Research Letters*, 1-10, https://doi.org/10.1785/0220200207

Papazachos B. C., Savvaidis, A. S., Papazachos K., Papaioannou, C., Kiratzi, A., Muco, B., et al. (2001). Atlas of Isoseismal Maps for Shallow Earthquakes in Albania and surrounding Area (1851-1990). *Geophysical Laboratory Aristotle University Thessaloniki*, 74, doi: 10.13140/RG.2.1.1050.2487

RCMT, European-mediterranean Regional Centroid Moment Tensor (RCMT) Catalog, Available from: http://rcmt2.bo.ingv.it/ (Accessed on 15 May 2020)

Rosen, P. A., Gurrola, E. M., Agram, P., Cohen, J., Lavalle, M., Riel, B. V., et al. (2018). The InSAR scientific computing environment 3.0: A Flexible Framework for NISAR Operational and User-led Science Processing. Paper presented at *IEEE International Geoscience and Remote Sensing Symposium* (IGARSS 2018), Piscataway, NJ, USA, 4897-4900, https://doi.org/10.1109/IGARSS.2018.8517504

Schimd, S. M., Bernoulli, D., Fugenschuh, B., Matenco, L., Schefer, S., Schuster, R., et al. (2008). The Alpine-Carpathian-Dinaridic orogenic system: correlation and evolution of tectonic units. *Swiss Journal of Geosciences*, 101, 139-183, https://doi.org/10.1007/s00015-008-1247-3

Schmid, S. M., Fugenschuh, B., Kounov, A., Matenco, L., Nievergelt, P., Oberhansli, R., et al. (2020). Tectonic units of the Alpine collision zone between Eastern Alps and western Turkey. *Gondwana Research*, 78, 308-374, https://doi.org/10.1016/j.gr.2019.07.005

Serpelloni, E., Facenna, C., Spada, G., Dong, D., & Williams, S.D.P., (2013). Vertical GPS ground motion rates in the Euro-Mediterranean region: new evidence of velocity gradients at different spatial scales along the Nubia-Eurasia plate boundary. *Journal of Geophysical Resesearch: Solid Earth*, 118(11), 6003–6024, https://doi.org/10.1002/2013JB010102

Silo, V., Nishani, P., & Silo, E. (2010). Hydrocarbon exploration under Kruja zone in Tirana-Rodon area Albania. *Journal of the Balkan Geophysical Society*, 10 (1), 9 -16

Stucchi, M., Rovida, A., Gomez Capera, A. A., Alexandre, P., Camelbeeck, T., Demircioglu, M. B., et al. (2013). The SHARE European Earthquake Catalogue (SHEEC) 1000-1899. *Journal of Seismology*, 17, 523-544, https://doi.org/10.1007/s10950-012-9335-2

USGS, U.S. Geological Survey (USGS), Earthquake Catalog, Available from: https://earthquake.usgs.gov/earthquakes/search/ (Accessed on 15 May 2020)

Velaj, T. (2015). New ideas on the tectonic of the Kurveleshi anticlinal belt in Albania, and the perspective for exploration in its subthrust, *Petroleum*, 1(4), 269-288, https://doi.org/10.1016/j.petlm.2015.10.013

Xhomo, A., Kodra, A., Dimo, L.I., Gjat, K., Xhafa, Z.,et al. (1999). Tectonic Map of Albania (1:200.000). Tirana, Ministry of Industry and Energy, Ministry of Education and Science, Albanian Geological Survey, AlpPetrol, Polytechnical University of Tirana

Xhomo, A., Kodra, A., Dimo, L.I., Xhafa, Z., Nazaj, S.H., et al. (2002). Geological Map of Albania (1:200.000). Tirana, Ministry of Industry and Energy, Ministry of Education and Science, Albanian Geological Survey, AlpPetrol, Polytechnical University of Tirana

Yu, C., Li, Z., Penna, N. T., & Crippa, P. (2018). Generic atmospheric correction model for Interferometric Synthetic Aperture Radar observations. *Journal of Geophysical Research: Solid Earth*, 123(10), 9202-9222, https://doi.org/10.1029/2017JB015305

Figure 1.

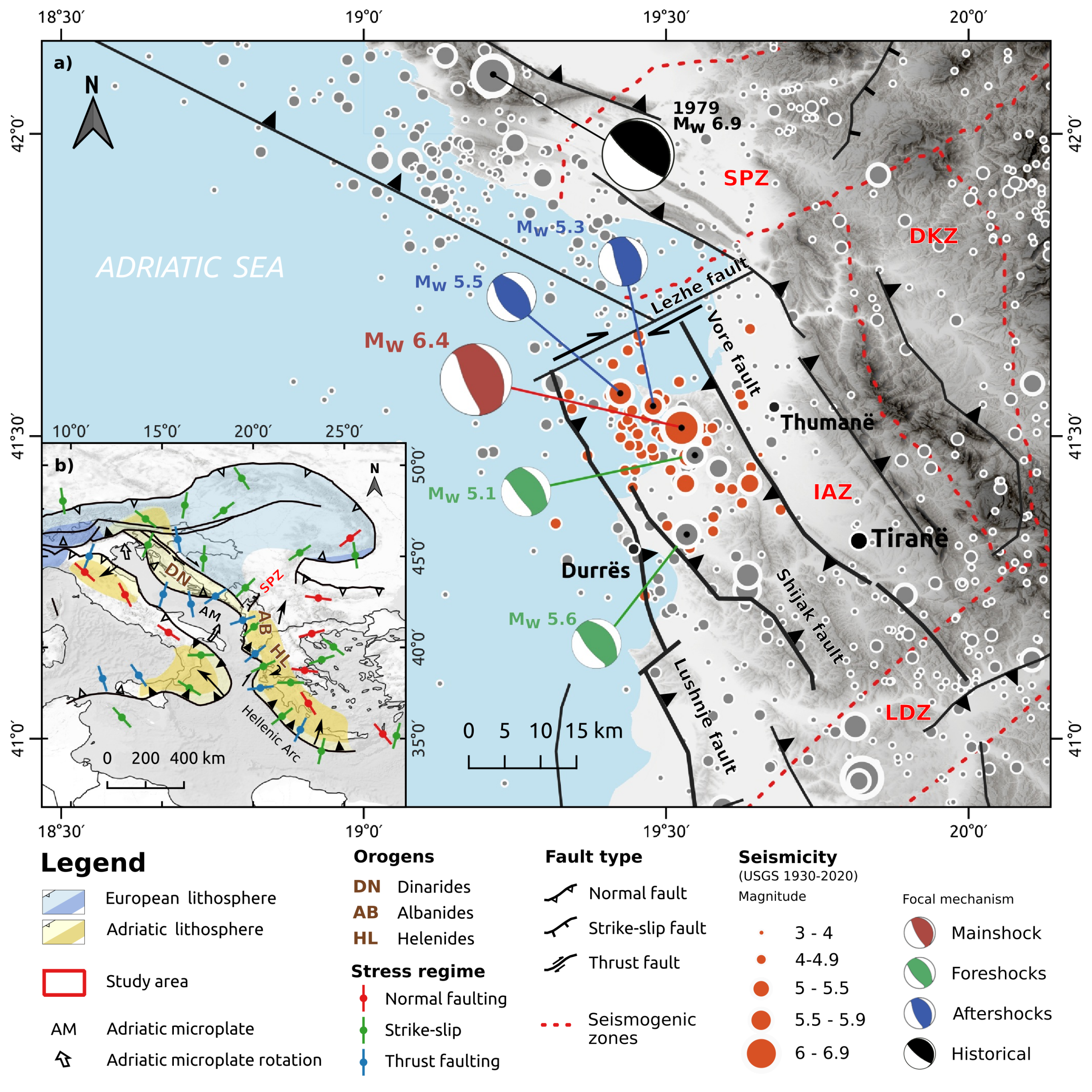
18°30′
19°0′
19°30′
20°0′
42°0′
41°30′
41°0′
a)
N
1979
Mw 6.9
SPZ
DKZ
IAZ
LDZ
ADRIATIC SEA
Mw 5.3
Mw 5.5
Mw 6.4
Mw 5.1
Mw 5.6
Lezhe fault
Vore fault
Thumanë
Tiranë
Durrës
Shijak fault
Lushnje fault
0 5 10 15 km
b)
10°0′
15°0′
20°0′
25°0′
50°0′
45°0′
40°0′
35°0′
DN
AB
HL
AM
SPZ
Hellenic Arc
0 200 400 km
Legend
European lithosphere
Adriatic lithosphere
Study area
AM Adriatic microplate
Adriatic microplate rotation
Orogens
DN Dinarides
AB Albanides
HL Helenides
Stress regime
Normal faulting
Strike-slip
Thrust faulting
Fault type
Normal fault
Strike-slip fault
Thrust fault
Seismogenic zones
Seismicity
(USGS 1930-2020)
Magnitude
3 - 4
4-4.9
5 - 5.5
5.5 - 5.9
6 - 6.9
Focal mechanism
Mainshock
Foreshocks
Aftershocks
Historical

Figure 2.

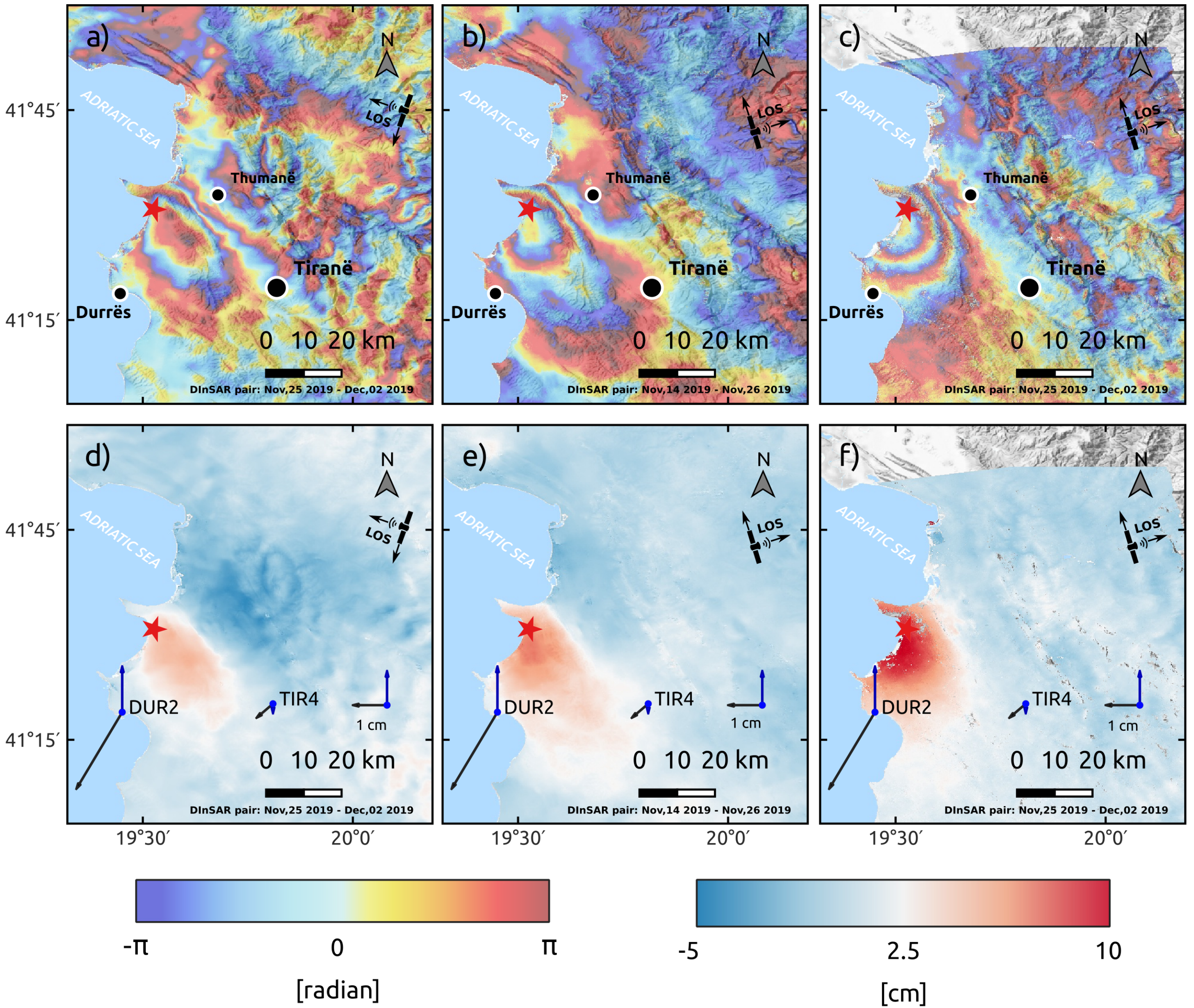

a)
b)
c)
d)
e)
f)
N
LOS
ADRIATIC SEA
Thumanë
Tiranë
Durrës
DUR2
TIR4
1 cm
0 10 20 km
DInSAR pair: Nov,25 2019 - Dec,02 2019
DInSAR pair: Nov,14 2019 - Nov,26 2019
41°45′
41°15′
19°30′
20°0′
-π
0
π
[radian]
-5
2.5
10
[cm]

Figure 3.

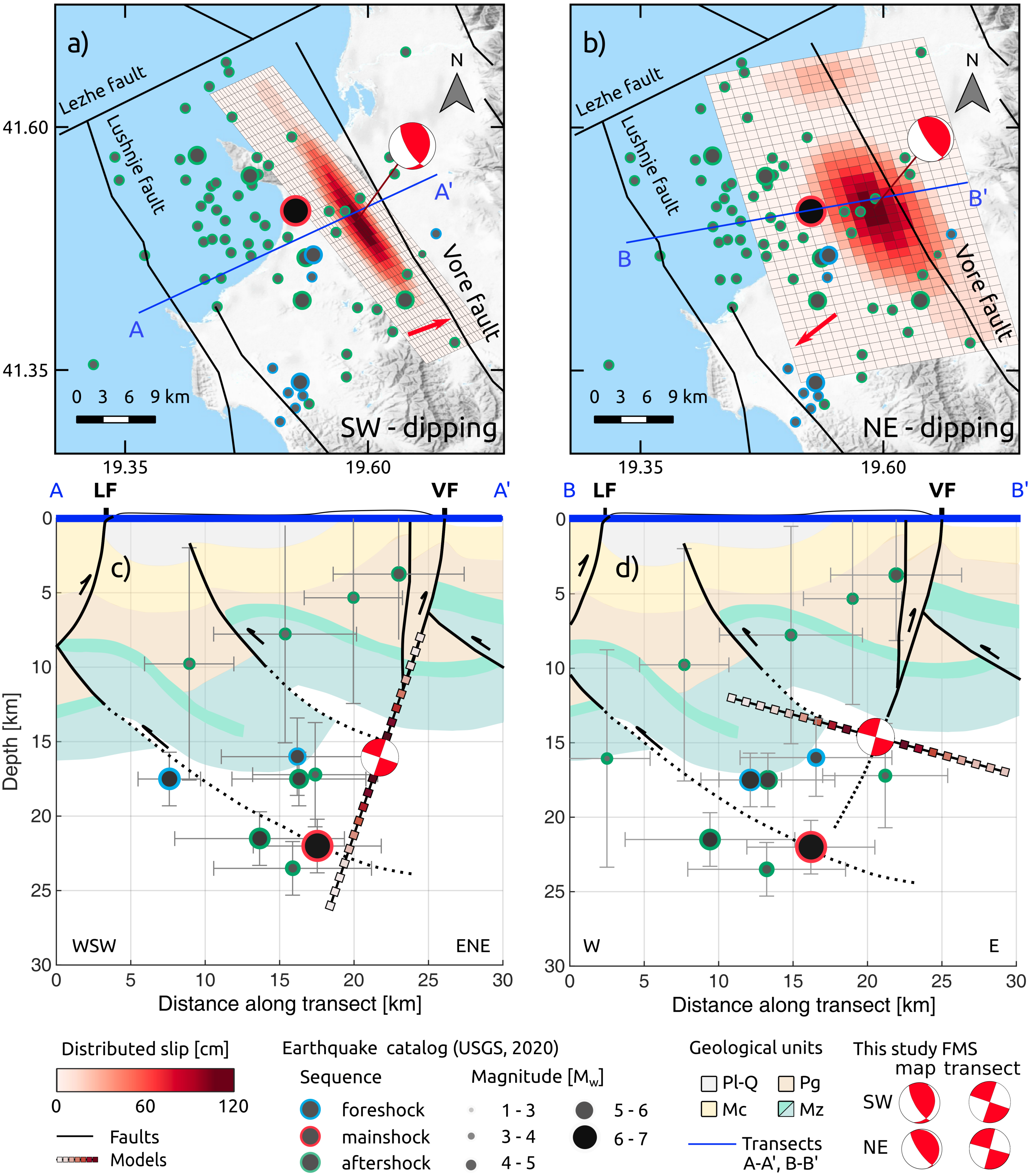

a)
b)
Lezhe fault
Lushnje fault
Vore fault
N
A
A'
B
B'
41.60
41.35
19.35
19.60
0 3 6 9 km
SW - dipping
NE - dipping
c)
d)
LF
VF
WSW
ENE
W
E
Depth [km]
Distance along transect [km]
Distributed slip [cm]
0
60
120
Faults
Models
Earthquake catalog (USGS, 2020)
Sequence
foreshock
mainshock
aftershock
Magnitude [Mw]
1 - 3
3 - 4
4 - 5
5 - 6
6 - 7
Geological units
Pl-Q
Pg
Mc
Mz
Transects A-A', B-B'
This study FMS
map transect
SW
NE